Article

Design of Model-Based and Model-Free Robust Control Strategies for Lower Limb Rehabilitation Exoskeletons

Muhammad Tallal Saeed [1,2,*] ![ORCID], **Jahan Zeb Gul** [2] ![ORCID], **Zareena Kausar** [2] ![ORCID], **Asif Mahmood Mughal** [3], **Zia Mohy Ud Din** [2] **and Shiyin Qin** [1]

1   Department of Intelligent Systems and Control Engineering, School of Automation Science and Electrical Engineering, Beihang University, Beijing 100191, China; qsy@buaa.edu.cn
2   Department of Mechatronics and Biomedical Engineering, Air University, Islamabad 44230, Pakistan; jahanzeb@mail.au.edu.pk (J.Z.G.); zareena.kausar@mail.au.edu.pk (Z.K.); drzia@mail.au.edu.pk (Z.M.U.D.)
3   Department of Electrical and Computer Engineering, Sir Syed Center for Advanced Studies in Engineering and Information Technology, Islamabad 45211, Pakistan; asifm@case.edu.pk
*   Correspondence: talalsaeed@buaa.edu.cn; Tel.: +92-344-547-8471

Featured Application: Precise and accurate lower limb rehabilitation in the form of locomotion assistance and gait training through robust control of robotic exoskeletons.

Abstract: Rehabilitation in the form of locomotion assistance and gait training through robotic exoskeletons requires both precision and accuracy to achieve effective results. The essential challenge is to ensure robust tracking of the reference signal, i.e., of the gait or locomotion. This paper presents the design of model-based (MB) and model-free (MF) robust control strategies to achieve desired performance and robustness in terms of transient behavior and steady-state/tracking error, implementable to the locomotion assistance and gait training by exoskeletons. The dynamic responses of the exoskeleton system were investigated with both the control strategies. The study was carried out with a variety of reference signals and performance was evaluated to identify the best suited approach for rehabilitation exoskeletons. In case of the model-based control, a mathematical model of the system was developed using a bond graph modeling technique and a lead compensated H-infinity reference gain controller was designed to ensure robust tracking performance. In the model-free control strategy, however, the system function is approximated using radial basis function neural networks (RBFNNs) and an adaptive proportional-derivative RBFNN controller was designed to achieve the desired results with minimum tracking error. Both strategies make the system robust and stable. However, the MF control strategy is faster for all reference inputs as compared to the MB control strategy i.e., faster to approach the peak value and settle, and rapidly approaches the zero steady-state/tracking error. The rise time in the case of a sinusoidal input for model-free control is 0.4 s faster than the rise time in model-based control. Similarly, the settling time is 3.9 s faster in the case of model-free control, which is a prominent difference and can provide better rehabilitation results.

Keywords: bond graph modeling; model-based control; rehabilitation; exoskeleton; robust reference tracking

1. Introduction

Natural mobility hindrance for human beings is a critical problem as it causes dependency and poor quality of life. This hindrance is caused by physiological (muscular or skeletal) or neurological disorders or disabilities (stroke, spinal cord injuries etc.) [1]. In recent years, the use of robotic exoskeletons in the medical field for lower limb rehabilitation has gained much importance throughout the world. This is mainly because of two reasons: firstly, unlike passive conventional mobility aids (such as crutches, manual wheelchairs, and walkers etc.), exoskeletons are a source of active anthropomorphic

mobility. Secondly, exoskeletons support rehabilitation in the form of locomotion assistance and gait training. In both forms, exoskeletons are proven to be more beneficial and effective in terms of comfort and results, as compared to conventional assistance and manual training [2,3]. For these reasons, more research has been carried out in the field of rehabilitation exoskeletons and numerous multidisciplinary (electrically, hydraulically, or pneumatically powered) exoskeletons have been designed [1,4,5]. Whether designed for active or passive rehabilitation, a state-of-the-art mechanical design requires an effective control strategy to provide desired performance. Active rehabilitation refers to repetitive movements/exercises through exoskeletons with assist-when-required algorithms, either integrated with trajectory tracking or repetitive learning. This ensures active participation of the patient, whereas passive rehabilitation involves reference/trajectory tracking control of the robotic exoskeleton, i.e., the control law is designed to ensure proper tracking of a pre-defined reference/trajectory. The patient forcibly receives training. Passive rehabilitation training mostly uses trajectory tracking, whereas the active rehabilitation training employs impedance control with assist-when-required algorithms. This research focuses on passive rehabilitation through exoskeletons and provides control strategies that ensure trajectory tracking over a predefined gait pattern.

The reference trajectory tracking controllers are broadly categorized as model-based (MB) and model-free (MF) controllers. A model-based control strategy requires mathematical modeling of the system; however, a model-free controller does not need an exact mathematical model, but a system function is approximated. The lower limb exoskeletons are modeled as a two link [6,7] or three link [8,9] manipulator. In most of the previous research, the Lagrange method is used for development of the mathematical model of system dynamics. This method uses the difference between the kinetic and potential energies acting on the links, and derives a dynamics model of the system in the form of a relationship between the associated force/torque and the generalized coordinates. The standard form of dynamics of a mechanism is expressed as Equation (1):

$$\tau = M(q)\ddot{q} + C(q,\dot{q}) + G(q) \tag{1}$$

where $\tau \in R^n$ is the applied torque, $M(q) \in R^n$ is the inertia matrix, $C(q,\dot{q}) \in R^n$ represents Coriolis and centrifugal force, $G(q) \in R^n$ is the gravitational force, and $q \in R^n$ denotes the angle. Equation (1) can be modified with addition of external disturbances 'd' (refers to the interference that becomes part of the system exogenously) at the system input [10] and model uncertainties 'Δ' (refers to difference between the actual system and the modeled system) [11,12]. The resulting modification is shown in Equation (2):

$$\tau = M(q)\ddot{q} + C(q,\dot{q}) + G(q) + \Delta + d \tag{2}$$

The Lagrangian approach in the case of systems having complex dynamic characteristics requires more computations. An alternate approach for modeling the manipulators is the bond graph. The bond graph technique provides a model of the system with less complexity and more flexibility [13,14], as compared to the conventional Lagrangian method [15,16]. Hence, the bond graph technique was used in this study for the modeling of exoskeleton for rehabilitation. Similar studies in which a bond graph is used to model a powered exoskeleton for use as an industrial backpack and a knee joint exoskeleton are presented in [17,18].

It is worth mentioning that rehabilitation in the form of locomotion assistance and gait training through robotic exoskeletons requires both precision and accuracy. The essential challenge for this is to ensure robust tracking of the desired trajectory of locomotion. This desired trajectory is basically a clinical gait pattern provided by the physician, and the exoskeleton as a rehabilitation equipment is used and controlled to ensure that the patients repetitively follow the pattern to train or exercise the muscles. The control strategies used in the literature for trajectory tracking are designed either using the model of the system [19–33], the approximated function [34–44], or the combination of both [6]. To

ensure tracking, various types of controllers are used. In some cases, a single control action is enough to fulfil the required task but, in other cases, a combination of one or more controllers is required. Trajectory tracking through impedance/admittance control is also carried out [19–22] where the impedance between the exoskeleton and the human leg is controlled by changing the force applied by the actuator. MB and MF trajectory tracking control strategies are also used to achieve reference signal tracking in exoskeletons, with high stability and performance.

In [23], a MB sliding mode controller is designed. The results show that all three joints reach the desired set angles in simulation but in experimentation the hip and knee joints do not reach the final value. Similarly, a pneumatic muscle-based two-DOF ES is controlled by proportional-derivative (PD) and adaptive control strategies separately in [7]. The results show that the output is slightly out of phase for PD control but for adaptive control the tracking results show adaptation within 1.5 s of operation. There exists an initial error of 1 for both the joint angles. Trajectory tracking through adaptive sliding mode impedance control is implemented in [24]. The results show better tracking for the knee joint but for the hip joint there is a delay in phase. The work presented in [45] focuses on achieving system robustness and dynamic performance similar to that of this research, for a 2-DOF LLE. An MB robust sliding mode controller is designed to achieve the desired output.

A new classical PD and PD-particle swarm optimization augmented force control (PSOAFC) approach is implemented in [25]. There exists phase delay in joint angles in the case of a time-varying signal. However, for a simple model with an external disturbance torque vector, PD-PSOAFC shows better results than classical PD. In other research works for passive rehabilitation, the MB controllers designed for trajectory tracking include an adaptive admittance control for unstructured uncertainty compensation [26], a sliding mode controller for robustness [28,31], and an intelligent adaptive fuzzy approach [33]. In a model-free control strategy, however, the mathematical model is not derived, and the system is presented in the form of a function. This function is approximated using techniques such as system identification and artificial intelligence. Model-free control strategies for efficient tracking performance have been designed in various studies, most of which used neural networks to approximate the function of the system and the control law design. The MF controllers designed for passive rehabilitation include an intelligent adaptive controller [34,41,42], an intelligent robust controller [35,40], and a second-order robust sliding mode controller [39].

These MB and MF trajectory tracking control strategies perform well. However, they also present some issues, including tracking error range, output being out of phase from input, non-robust performance in the presence of disturbances, and parametric uncertainties. This research, therefore, focuses on the enhancement of tracking performance of the LLRE in the presence of disturbances and uncertainties, and elimination of phase delay, especially in the case of a time-varying reference signal. This is achieved via the design of both the MB and MF robust control strategies. The performance of both of the closed loop systems was analyzed to identify the optimized robust control methodology for the LLRE. The paper is divided into five sections, including the introduction given in Section 1. In Section 2, the design of the model-based control strategy is presented and the simulation results are analyzed. In the following section, the design of the model-free control strategy and the simulation results are presented. A comparative analysis of results is presented in Section 4 to identify the optimized methodology for robust control of the LLRE, before the study is concluded in Section 5. See Figure 1.
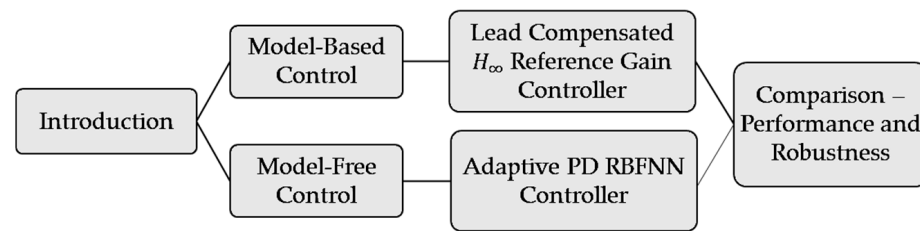
Figure 1. Research flow.
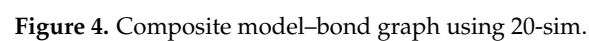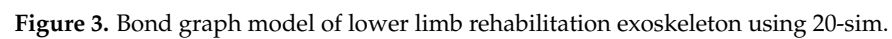
2. Model-Based Robust Control Design

This section presents the design of a model-based control strategy to address the robust control problem and to ensure the tracking of the reference time-varying harmonic signal. The robust control problem is formulated such that there exist input and output disturbances and unstructured additive mismatched uncertainty at the inertial mass of the lower limb exoskeleton links, including the human leg, which an exoskeleton undergoes during rehabilitation process. The mathematical model of the system was developed using the bond graph modeling technique. This research work is an extension of our previous work presented in [13,46]. Previously, the designed MB control law provided disturbance rejection and uncertainty compensation but the final value in case of step and impulse inputs was not achieved. Secondly, the control law for a time-varying periodic signal was not designed. Here, first, the control law was modified to achieve a final value with a zero steady-state. Second, the control law was upgraded to provide reference tracking in the case of a sinusoidal input.

2.1. Mathematical Model Using Bond Graph

A mathematical model of the three-link exoskeleton manipulator, in the form of a transfer function and state space equations, was obtained using the bond graph modeling technique as given in (3) and (4). A schematic diagram of the exoskeleton and the bond graph model of the system generated using the 20-sim software are presented in Figures 2 and 3, respectively. For the control of link_1, associated with the hip joint, a composite model is required because, during the locomotion assistance and gait training, the motor at the hip joint (mhj), including the inertial mass, stiffness, and viscous friction associated with link_1, experiences the effect of the remaining structure, i.e., two motors (the motor at the knee joint (mkj) and the motor at the ankle joint (maj)), two links, and the human leg except the thigh, as a mass-spring-damper load [13,46]. Similarly, the actuator at the knee joint is influenced by the third motor and third link in the form of a mass-spring-damper load. Hence, for the velocity control of the first link, a composite model can be realized with the combined masses of the remaining two actuators (motor_2 and motor_3), links (link_2 and link_3), and the mass of the remaining human leg, considered at link_1 (as $I : Mass\_lftfftlfot$). Similarly, combined damping, stiffness, and gravitational force associated with link_2 and link_3 are considered at link_1 (as $R : Fv\_fftjftfotjfotgd$, $C : Ks\_fftjftfotjfotgd$, and $Se : g\_Masslftfftlfot$), respectively, as shown in Figure 4. A composite model obtained as the mathematical model to control the position of link_1 is presented in Figure 4. The description of variables of the bond graph [13] of the composite model, and the transfer function of the composite model defining a relationship between the applied input voltage (E) and the link velocity (V) of link_1 with the combined effect at the output, are presented in Table 1 and Equation (3), respectively.

$$G_P(s) = \frac{V(s)}{E(s)} = \frac{5e^5s + 1250}{s^5 + 100s^4 + 1.461e^4s^3 + 2.1e^5s^2 + 1.256e^6s + 3125} \tag{3}$$

Figure 2. Schematic diagram of lower limb rehabilitation exoskeleton.

Figure 3. Bond graph model of lower limb rehabilitation exoskeleton using 20-sim.

Figure 4. Composite model–bond graph using 20-sim.

State space realization is presented in Equation (4).

$$\left.\begin{array}{c} \dot{x} = Ax + Bu \\ y = Cx \end{array}\right\} \qquad (4)$$

Such that:

$$A = \begin{bmatrix} -100 & -250 & 0 & 0 & 0 \\ 50 & -0.003664 & 0 & -20 & 0 \\ 0 & 0 & -0.0025 & 0 & -0.1 \\ 0 & 100 & 0 & 0 & 0.1 \\ 0 & 0 & -1.002e^{-6} & 100 & 0 \end{bmatrix}, \ B = \begin{bmatrix} 1 \\ 0 \\ 0 \\ 0 \\ 0 \end{bmatrix}$$

$$C = \begin{bmatrix} 0 & 0 & 0 & 0 & 0.1 \end{bmatrix}$$

$$x = \begin{bmatrix} x_{Ia\_mhj} \\ x_{Jasft\_mhj} \\ x_{Ksfftjftfotjfotgd} \\ x_{Ksnt\_mhj} \\ x_{Mass\_lftfftlfot} \end{bmatrix} = \begin{bmatrix} \text{Armature Current}^* \\ \text{Moment of Inertia of Armature Shaft}^* \\ \text{Composite K between Joints and Ground} \\ \text{Spring Constant of Nut}^* \\ \text{Mass of all links} \end{bmatrix}$$

$$* : Motor\ at\ Hip\ Joint$$

2.2. Robust Optimization Problem and Control Design

The position control problem is formulated as a robust optimization problem. The disturbances and the uncertainty are introduced in the system, and the control law is then designed to achieve tracking. The salient points of the control problem are presented in the following.

2.2.1. Input/Output Disturbance

Input and output disturbances that an exoskeleton undergoes during the rehabilitation process are added to the model. Input disturbance is introduced in the system as a fluctuation in the applied voltage. Output disturbance is considered as the unintentional continuous force applied by the patient during the passive rehabilitation. More details regarding the disturbances can be found in [46].

2.2.2. Additive Mismatched Uncertainty

Uncertainty is referred as the possible difference in parametric values of a modeled plant compared to the actual plant. This may be because of un-modeled system dynamics or a known bounded perturbation in a system parameter. For the LLRE, one possible unstructured uncertainty added refers to the difference in the inertial mass of the three links and the human leg compared to the modeled inertia in the mathematical model. The state variable $x_{Mass\_lftfftlfot}$ (fifth state) represents the inertial mass and a value of 0.01 is added as a perturbation Δx in this state, representing the additive uncertainty.

2.2.3. Controller Design

For the problem formulated above, an H_∞ controller [47,48] integrated with a lead compensator and a reference gain is proposed for the design to achieve robust output and desired performance.

The control scheme is presented in Figure 5. H_∞ control ensures disturbance rejection and uncertainty compensation for reference signals, but there remains a steady-state error for step and impulse inputs, and tracking error in the case of sinusoidal input.

Table 1. Variables of the composite model and their details.

Variable	Component	Description	Value
Se: e_mhj	Electrical	Source of Effort, i.e., Voltage Source	12 V
R: Ra_mhj	Electrical	Armature Resistance (Ra) of Linear Actuator	1 Ω
I: Ia_mhj	Electrical	Armature Inductance (Ia) of Linear Actuator	1 mH
GY: Gyration_Ratio_mhj	Mechanical	Gyration Ratio	5×10^{-2}
R: Dasft_mhj	Mechanical	Damping of the Armature Shaft (sft)	5.7286×10^{-7} Ns/m
I: Jasft_mhj	Mechanical	Moment of Inertia of Armature Shaft (sft)	2×10^{-4} kgm^2
TF: al_mhj	Mechanical	Angular to Linear (al)	2×10^{-2}
R: Fvsftnt_mhj	Mechanical	Viscous Friction between Shaft (sft) and Nut (nt)	1×10^{-4} Ns/m
C: Ksnt_mhj	Mechanical	Spring Constant of Nut (nt)	$1 \times 10^{+5}$
R: Fv_fftjftfotjfotgd	Mechanical	Viscous Friction between joints (Femur (f), Fibula and Tibia (ft), Foot (fot) and with ground (gd)	1×10^{-4} Ns/m
I: Mass_lftfftlfot	Mechanical	Mass of remaining actuators, links (l), and human leg	10
C: Ks_fftjftfotjfotgd	Mechanical	Spring Constant of remaining actuators, links and human leg	1×10^{-4}
Se: g_Mass lftfftlfot	Mechanical	Gravitational Force (g) associated with remaining structure	98
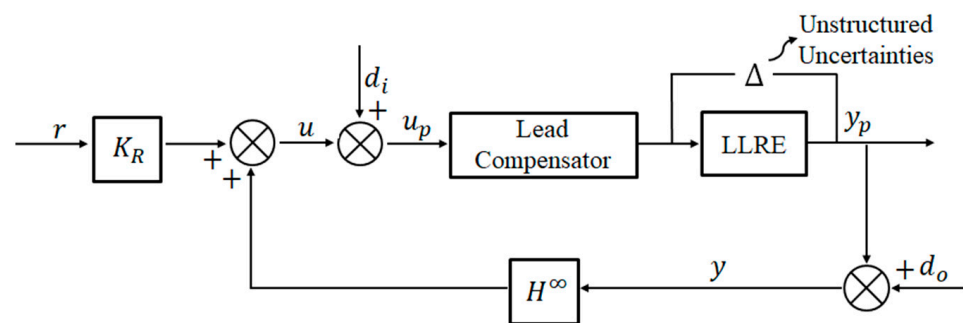
Figure 5. Lead-compensated H_∞ reference gain controller.

Remark 1. *The H_∞ controller ensures.*

- *Internal stability of the closed loop system*
- *$\|T_{z\omega}(s)\| < \gamma$ where, γ is a specified number < 0*

Remark 2. *The compulsory assumptions for the controller design are checked. These include:*

- *(A, B_2) is stabilizable and (A, C_2) is detectable*
- *Rank of matrix $\begin{bmatrix} A - \omega jI & B_2 \\ C_1 & D_{12} \end{bmatrix}$ should be full column rank and rank of matrix $\begin{bmatrix} A - \omega jI & B_1 \\ C_2 & D_{21} \end{bmatrix}$ should be full row rank*
- *For proper and realizable controller: Rank of D_{12} is full column rank and rank of D_{21} is full row rank.*

Remark 3. *The algorithm steps for the controller design followed are:*

- *The system is realized in the form of state space and the status of assumptions are checked to be satisfactory.*
- *A large positive value for γ is selected and the controller $K(s)$ is found after solving the Algebraic Riccati Equations (AREs) until a satisfactory solution is obtained, i.e., subject to the fulfilment of the following condition with lowering γ:*

$$\rho(X_\infty, Y_\infty) < \gamma^2$$

where X_∞ and Y_∞ are the solutions of the AREs.

- *The control law design takes the form; $u = -k_C \hat{x}(t)$. The reference gain is adjusted to achieve acceptable steady-state response/outcome for the step and impulse inputs but for the sinusoidal signal a phase delay exists in the output.*

A lead compensator is proposed to be integrated with the H_∞ controller to overcome the phase delay. The lead compensator is a passive network used to overcome the disadvantages of ideal differentiation and still retain the ability to improve the transient response. The standard form of the lead compensator is given in Equation (5):

$$G_C(s) = \frac{1}{\beta}\left(\frac{s + \frac{1}{T}}{s + \frac{1}{\beta T}}\right) \tag{5}$$

where $\beta < 1$. The control design assumptions for the H_∞ controller gain were checked and controller $K_C(s)$ is obtained by following the algorithmic steps. The feedback configuration of the controlled plant was simulated in MATLAB®. The test bound for γ is set as given in Equation (6):

$$0.0001 < \gamma \leq 100 \tag{6}$$

After fifteen iterations, a satisfactory solution was obtained, and the value of gamma achieved is 0.0062. The value of $\beta = 2.75 \times 10^{-3}$ for the maximum phase shift φ_{max} through the designed compensator value 83.9962°. The lead compensator break frequencies $\frac{1}{T} = 0.025$ and $\frac{1}{\beta T} = 9.09$. Hence, the compensator is described as Equation (7):

$$G_C(s) = \frac{1}{2.75 \times 10^{-3}}\left(\frac{s + 0.025}{s + 9.09}\right) \tag{7}$$

A gain is added at the reference signal 'K_R' to adjust the tracking error for the sinusoidal signal. The control law takes the form:

$$u = -k_C \hat{x}(t) + k_R r \tag{8}$$

$$u_p = u + d_i \tag{9}$$

The compensator $G_C(s)$ is cascaded with the plant $G_P(s)$. The H_∞ controller ensures stability, and the combination of compensator and reference gain ensures transient and tracking performance.

2.2.4. Simulation Results

Simulation results of the closed loop step, impulse, and sinusoidal responses of the closed loop system are presented in Figure 6. Locomotion and gait training involves signals with a closed loop response of the position, and the velocities of link_1 parallel to the femur bone of the human leg for the step, impulse, and sinusoidal reference signals are presented in Figure 6.
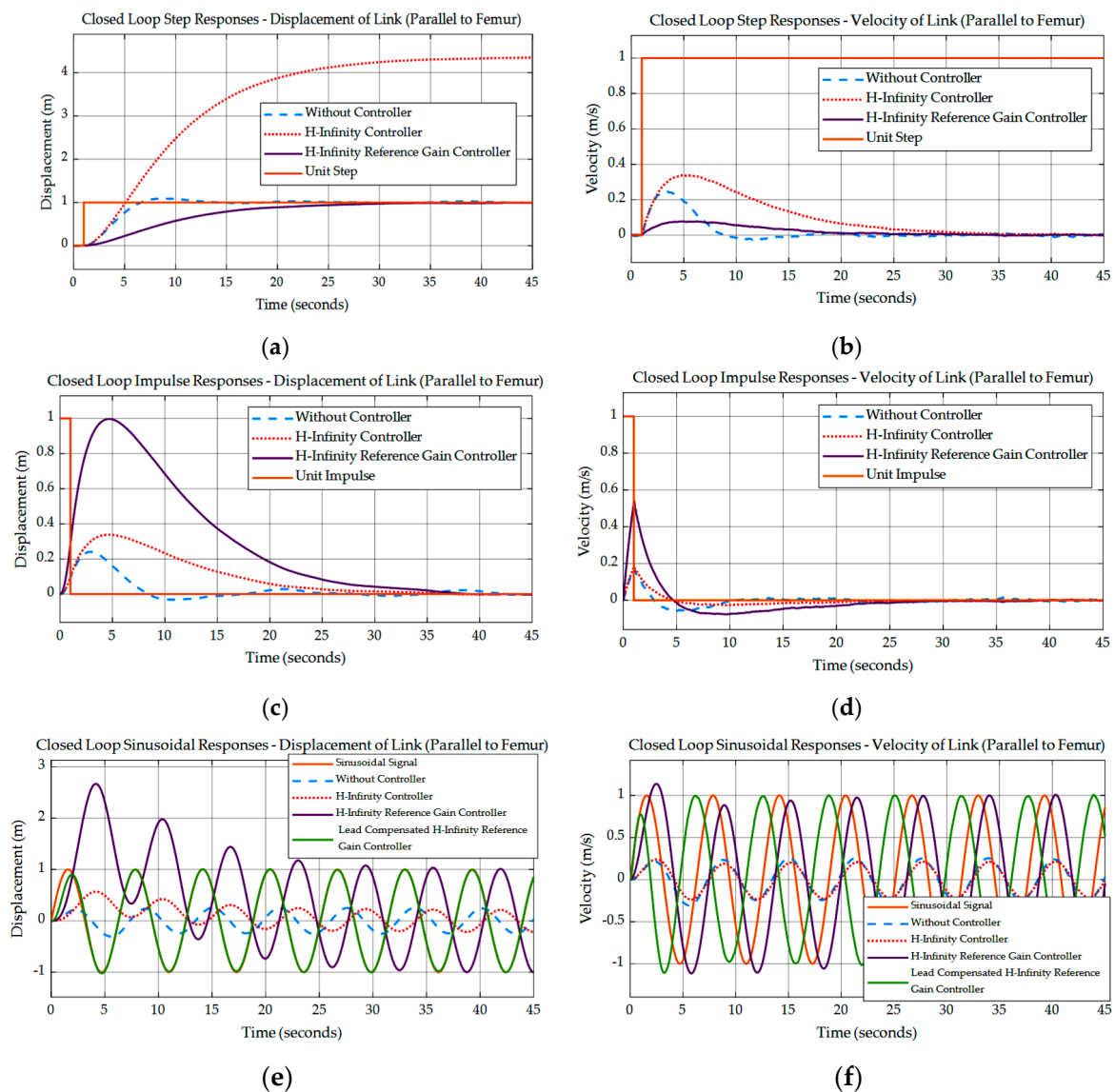
Figure 6. Model-based robust control design-closed loop responses of link (parallel to femur) (**a**) step responses—displacement; (**b**) step responses—velocity; (**c**) impulse responses—displacement; (**d**) impulse responses—velocity; (**e**) sinusoidal responses—displacement; (**f**) sinusoidal responses—velocity.

3. Model-Free Robust Control Design

This section presents the design of reference tracking control of the LLRE using the model-free strategy. The un-modeled dynamic components of both subsystems of the LLRE (electrical and mechanical), exogenous and endogenous disturbances, and mismatched unstructured uncertainties are represented as a single lumped function f_{lpd} and the exoskeleton is presented in the form of a mathematical equation as Equation (8):

$$x_{mf}^{(i)} = f_{lpd}(x) + \alpha v \tag{10}$$

In Equation (8), $x_{mf}^{(i)} \in R^n$ is the acceleration of the stroke of the linear actuator and i represents the derivative, which is taken as 2, $v \in R^n$ is the applied voltage to the actuator,

and α is the scaling factor of the input. Equation (8) is realized in the state space form as Equation (9):

$$\left.\begin{array}{c} \dot{x}_{mf_1} = x_{mf_2} \\ \dot{x}_{mf_2} = f_{lpd}(x) + \alpha v \\ y = x_{mf_1} \end{array}\right\} \tag{11}$$

where $x_{mf_1} \in R^n$ is displacement of the link attached to the stroke of the linear actuator, $x_{mf_2} \in R^n$ is the velocity of the link, and y is output of the system.

The challenge is to design a robust controller with minimal steady-state/tracking error. To accomplish this challenge, there has been extensive research in designing a neural network (NN) approximation function-based controller and an NN system identification-based controller for both lower and upper limb exoskeletons [35,49,50]. Here, a MF adaptive controller was designed to achieve the desired performance.

3.1. Adaptive PD RBFNN Controller Design

A simple model-free realization of the system as a linear relationship between the input, i.e., voltage v applied to the linear actuator and output y, i.e., linear displacement x of the link of mass m is considered. The input voltage is applied to the actuator and link_1 undergoes a linear displacement. There exist external disturbances d at the input and output of the system and uncertainties Δ with bounds $(a \le \|\Delta\| \le b)$, $a, b \in R^n$ or un-modeled dynamics that are part of the system. For the realized model, a Lyapunov-based adaptive PD controller was designed to achieve robust reference tracking. There is no information about the lumped function $f_{lpd}(x)$, which is essential for the controller design. An RBFNN was used to estimate the function and, using this function $\hat{f}_{lpd}(x)$, the controller was designed. An adaptive PD RBFNN control loop is presented in Figure 7.
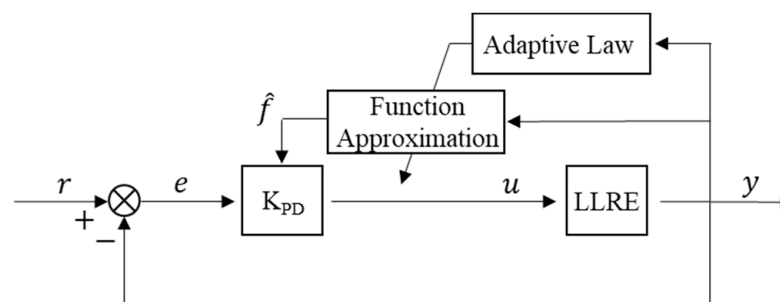
Figure 7. Adaptive PD RBFNN controller.

The desired position is stated as y_d and the error e (error between the desired output and the current output) can be formulated as

$$e = y_d - y = y_d - x_{mf_1} \tag{12}$$

$$E = \left[\begin{array}{cc} e & \dot{e} \end{array}\right]^T$$

Using Equation (10), the control law for the feedback configuration is formulated as:

$$\ddot{x}_{mf_1} = \alpha v + f_{lpd}(x) \tag{13}$$

$$\ddot{y}_d - \ddot{e} = \alpha v + f_{lpd}(x)$$

Using the intelligent PD control:

$$\ddot{e} + k_P e + k_D \dot{e} = 0 \tag{14}$$

$$\ddot{e} = -K^T E$$

$$v^* = \frac{1}{\alpha}\left\{-f_{lpd}(x) + \ddot{y}_d - \ddot{e}\right\}$$

$$v^* = \frac{1}{\alpha}\left\{-f_{lpd}(x) + \ddot{y}_d + K^T E\right\} \tag{15}$$

where $K^T = \begin{bmatrix} k_P & k_D \end{bmatrix}$.

In Equation (14), $f_{lpd}(x)$ is unknown, which is essential for the control law. $f_{lpd}(x)$ is approximated using the NN and is used to realize the control law.

3.1.1. Function Approximation

The RBFNN is used to approximate function $\hat{f}(x)$; the algorithm is described below:

$$f(x) = W^{*T}h(x) + \varepsilon \tag{16}$$

$$h_j = exp\left(\frac{\|x_i - c_{ij}\|^2}{b_j^2}\right) \tag{17}$$

where $x_i = [x_1 \ldots x_n]^T$, $n = 2$ is the input vector, $h_j = [h_1 \ldots h_m]^T$, $m = 5$ is the Gaussian function for neural net j (number of hidden layers) in hidden layer, $c = [c_{ij}] = \begin{bmatrix} c_{11} & \cdots & c_{1m} \\ \vdots & \ddots & \vdots \\ c_{n1} & \cdots & c_{nm} \end{bmatrix}$ represents the coordinate value of center point of the Gaussian function of neural net j for the ith input, $i = 1, 2, \ldots, n$, $j = 1, 2, \ldots, m$. $b_j = [b_1, b_2, \ldots, b_m]^T$, $m = 5$ represents the width value of the Gaussian function for neural net j, $W^{*T} = [w_1, w_2, \ldots, w_m]^T$, $m = 5$ is the ideal weight value of the RBF. ε is approximation error, $\varepsilon \leq \varepsilon_N$. The output of the RBF is presented in Equation (17):

$$\hat{f}_{lpd}(x) = \hat{W}^T h(x) \tag{18}$$

where $\hat{W}$ is the estimated weight vector which is tuned by the adaptive algorithm in the Lyapunov stability analysis.

3.1.2. Effects of Different Parameters on RBF Approximation

The RBF approximation is affected by different parameters. These include the Gaussian function (related to the design of the center vector c_j and width value b_j) and the number of hidden nets. There are principles for the design of c_j and b_j, the details of which are presented in [51].

After careful consideration, two inputs, five hidden layers, and one output RBF neural network structure $(2 - 5 - 1)$ were used; the details are presented below:

Inputs: $i = 2$.

In the control system, when RBF is used to approximate f, the system states are chosen as the input of the RBF neural network.

Output of Gaussian function for five hidden neural nets $(j = 5)$, $h_j = \begin{bmatrix} h_1 & h_2 & h_3 & h_4 & h_5 \end{bmatrix}$.

Using the principles to design c_j for the given input, the coordinate values of the center point of the Gaussian function of neural net j are defined as:

$$c_{ij} = c_{2 \times 5} = \begin{bmatrix} -1 & -0.5 & 0 & 0.5 & 1 \\ -1 & -0.5 & 0 & 0.5 & 1 \end{bmatrix}$$

Width vector of Gaussian function b_j, $b_j = [b_1, b_2, \ldots, b_m]^T = 1.20$

where $b_j > 0$ represents the width value of the Gaussian function for neural net j.

3.1.3. Lyapunov Stability Analysis

By submitting the control law in Equation (14), the closed loop system is expressed as:

$$\ddot{e} = -K^T E + \left\{ \hat{f}(x) - f(x) \right\} \tag{19}$$

Let:

$$A_{mf} = \begin{bmatrix} 0 & 1 \\ -k_p & -k_d \end{bmatrix}, B_{mf} = \begin{bmatrix} 0 \\ 1 \end{bmatrix}$$

Equation (18) can be rewritten as:

$$\dot{E} = A_{mf} E + B_{mf} \left\{ \hat{f}_{lpd}(x) - f_{lpd}(x) \right\} \tag{20}$$

Optimal weight value is $W^* = \arg\min\limits_{W \in \Omega} \left\{ \sup \left| \hat{f}_{lpd}(x) - f_{lpd}(x) \right| \right\}$.

Modeling Error: $\varepsilon = \hat{f}_{lpd}(x|\hat{W}) - f_{lpd}(x|W^*)$.

Equation (19) becomes:

$$\dot{E} = A_{mf} E + B_{mf} [\{ \hat{f}_{lpd}(x|\hat{W}) - f_{lpd}(x|W^*) \} + \varepsilon] \tag{21}$$

Using Equation (20):

$$\dot{E} = A_{mf} E + B_{mf} \{ (\hat{W} - W^*)^T h(x) + \varepsilon \} \tag{22}$$

Choosing the Lyapunov function as:

$$V = \frac{1}{2} E^T P E + \frac{1}{2\gamma} (\hat{W} - W^*)^T (\hat{W} - W^*) \tag{23}$$

where γ is a positive constant. $(\hat{W} - W^*)$ denotes the parameter estimation error and the matrix P is symmetric and positive definite, and satisfies the following Lyapunov equation:

$$A_{mf}^T P + P A_{mf} = -Q \tag{24}$$

with $Q \geq 0$. Finding $\dot{V}$:

$$\dot{V} = \dot{V}_1 + \dot{V}_2 \tag{25}$$

$$V_1 = \frac{1}{2} E^T P E$$

$$V_2 = \frac{1}{2\gamma} (\hat{W} - W^*)^T (\hat{W} - W^*)$$

Taking the derivative of V_1:

$$\dot{V}_1 = \frac{1}{2} \dot{E} P E + \frac{1}{2} E^T P \dot{E}$$

Rewriting Equation (20) as:

$$\dot{V}_1 = \frac{1}{2} \dot{E} P E + \frac{1}{2} E^T P \dot{E} \tag{26}$$

$$\dot{E} = A_{mf} E + M \tag{27}$$

where $M = B_{mf} \{ (\hat{W} - W^*)^T h(x) + \varepsilon \}$.

Submitting Equation (26) into Equation (25):

$$\dot{V}_1 = \frac{1}{2} E^T \left(A_{mf}^T P + P A_{mf} \right) E + \frac{1}{2} M^T P E + \frac{1}{2} E^T P M$$

Using Equation (24):

$$\dot{V}_1 = \frac{1}{2}E^T Q E + E^T P M$$

Submitting M into the above equation:

$$\dot{V}_1 = -\frac{1}{2}E^T Q E + (\hat{W} - W^*)^T E^T P B_{mf} h(x) + E^T P B_{mf} \varepsilon \tag{28}$$

Taking the derivative of V_2:

$$\dot{V}_2 = \frac{1}{\gamma}(\hat{W} - W^*)^T \dot{\hat{W}} \tag{29}$$

Substituting Equations (27) and (28) into Equation (24):

$$\dot{V} = -\frac{1}{2}E^T Q E + E^T P B_{mf} \varepsilon + \frac{1}{\gamma}(\hat{W} - W^*)^T \left\{ \dot{\hat{W}} + \gamma E^T P B_{mf} h(x) \right\} \tag{30}$$

The adaptive law is chosen as:

$$\dot{\hat{W}} = -\gamma E^T P B_{mf} h(x) \tag{31}$$

Substituting Equation (30) into Equation (29):

$$\dot{V} = -\frac{1}{2}E^T Q E + E^T P B_{mf} \varepsilon \tag{32}$$

Since $-\frac{1}{2}E^T Q E \leq 0$, considering the adaptive control system convergence analysis in [52], if the approximation error ε is made very small using the RBF, $\dot{V} \leq 0$ can be achieved.

In order to design an adaptive PD RBFNN, first, a Lyapunov-based adaptive PD control law was designed. The unknown lumped function is approximated using the RBFNN. The error with the desired position y_d is defined as $E = \begin{bmatrix} e & e^T \end{bmatrix}$ and the adaptive PD control law is formulated as:

$$v^* = \frac{1}{\alpha}\left\{ -f(x) + \ddot{y}_d + K^T E \right\} \tag{33}$$

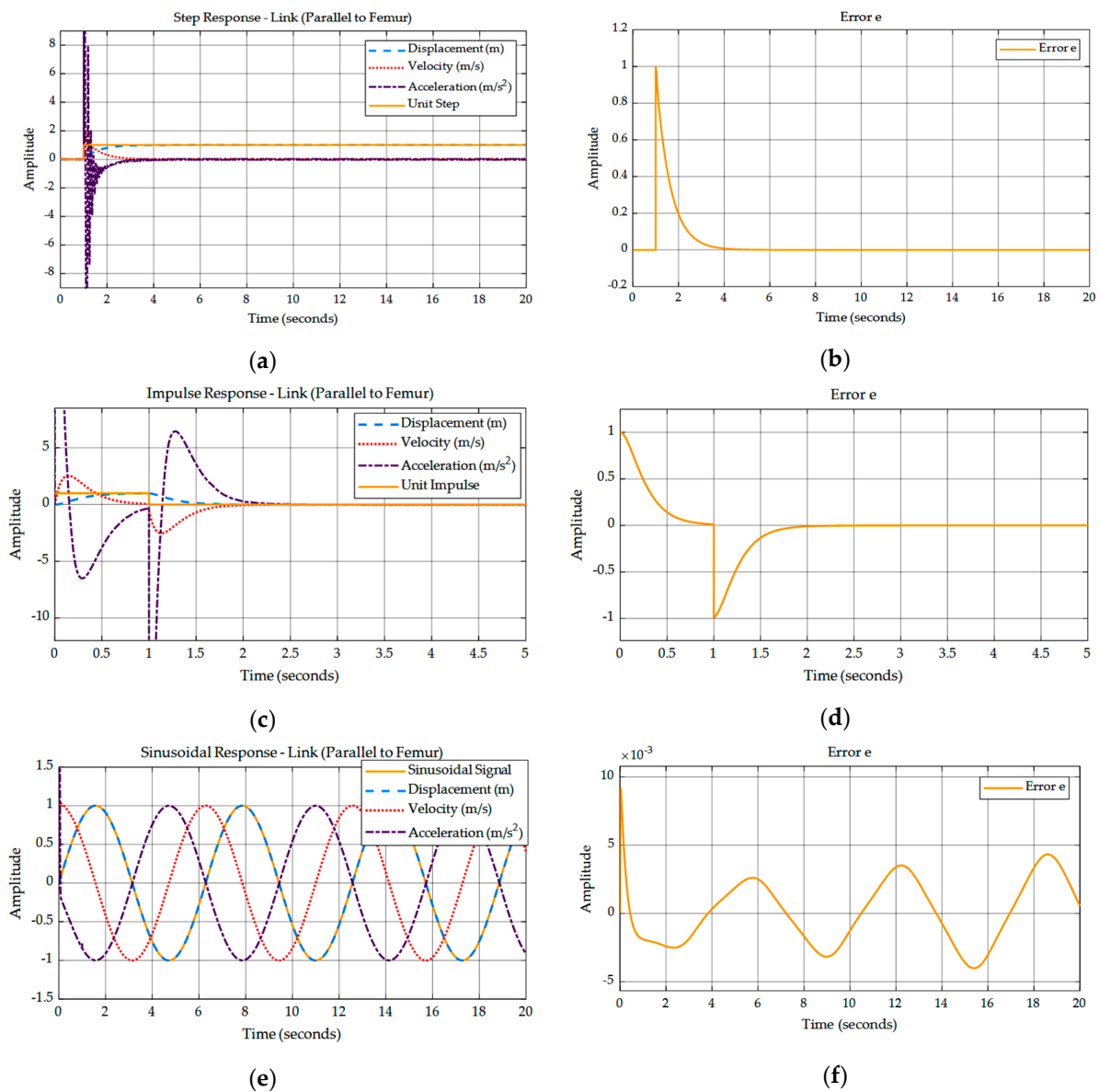where $K = \begin{bmatrix} k_P & k_D \end{bmatrix}$.

The adaptive law is defined as:

$$\hat{W} = -\gamma E^T P B_{mf} h(x) \tag{34}$$

3.1.4. Simulation Results

Dynamic responses of the controlled system for step, impulse, and sinusoidal inputs are shown in Figure 8. The adaptive PD controller was inspired by a research work [34], except that the additional neural network for estimation was removed.

Figure 8. Model-free robust control design-closed loop responses of link (parallel to femur) and tracking error: (**a**) step response-displacement, velocity, and acceleration; (**b**) tracking error displacement step response; (**c**) impulse response-displacement, velocity, and acceleration; (**d**) tracking error displacement impulse response; (**e**) sinusoidal response-displacement, velocity, and acceleration; (**f**) tracking error displacement sinusoidal response.

4. Results and Discussion

MB and MF robust control strategies were designed, and the simulation results are presented in the previous sections. The challenge to design MB and MF robust control strategies for achieving the desired performance in terms of transient behavior and steady-state error for step and impulse inputs, and minimizing the tracking error for a time-varying sinusoidal signal, was addressed successfully.

The step response of both the MB- and MF-controlled systems is robust as the system settles down in the presence of disturbances. However, the MF-controlled system settles faster as shown in Table 2. The same trend is followed in case of the impulse input. The slower system in the case of MB closed loop control is due to absence of a lead compensator. A lead compensator was not designed for these inputs because the objective to reach the desired final value was achieved without the effect of disturbances in these cases.

Table 2. Performance and Robustness-Displacement of Link_1 (Parallel to Femur).

Reference Signal	Performance and Robustness		
	Transient Behavior	Steady-State/Tracking Error	Robustness
Model-Based Control StrategyH_∞ Reference Gain Controller			
Step	Rise Time: 24 sPeak Value: 1Settling Time: 35 s	Minimized to Zero	Achieved
Impulse	Rise Time: 3.2 sPeak Value: 1Settling Time: 37 s	Minimized to Zero	Achieved
Sinusoidal	Rise Time: 3.2 sFirst Peak Value: 2.6Settling Time: 35 s	Output Signal Out-of-Phase from Input	Achieved
Model-Based Robust Control DesignLead Compensated H_∞ Reference Gain Controller			
Sinusoidal	Rise Time: 1.6First Peak Value: 0.8Settling Time: 4 s	Minimized to Zero within 4 s	Achieved
Model-Free Robust Control Design—Adaptive PD RBFNN Controller			
Step	Rise Time: 3.2 sSettling Time: 4.5 s	Minimized to Zero	Achieved
Impulse	Rise Time: 0.8 sSettling Time: 2 s	Minimized to Zero	Achieved
Sinusoidal	Rise Time: 1.2 sFirst Peak Value: 1Settling Time: 0.1 s	Minimized to Zero within 0.1 s	Achieved

In the case of a time-varying sinusoidal input, the response of the MB controller is relatively faster. This is because of the lead compensator integrated with the H_∞ reference gain controller. The lead compensator accounted for the delay in the reference input signal and the output signal. The sinusoidal input response of the MF-controlled system is faster than that of the MB controller. The results are summarized in Table 2.

The results show that, for both MB and MF controllers, the desired results, i.e., robustness and minimal steady-state/tracking error in the case of reference inputs, were achieved but the performance of the MF controller is better than that of the MB controller. The rise time and settling time are less in the case of MF control than that of MB control, indicating faster response. This work focused on achieving robustness for time-varying signals to achieve robustness in gait pattern tracking through the LLRE. The next step is to check the performance of the designed controllers for time-varying human gait patterns.

5. Conclusions

The challenge to design MB and MF robust control strategies to achieve desired performance for different inputs in terms of transient behavior and steady-state/tracking error is addressed. System modeling using the approach of the BG technique was carried out and simulation results were analyzed. System components responsible for resistance/damping, inductance/inertia, and capacitance/stiffness were considered for the LLRE to develop a precise model.

A model-based controller was then designed to address the robust control problem, which includes input and output disturbances, and un-modeled dynamics and uncertainties in the system, that cause poor control performance. The lead compensated H_∞ reference gain controller was proven to be a robust controller as it successfully attenuated the disturbances and, in the presence of uncertainty, provided the desired robust results. Before the integration of the lead compensator and the reference gain controller, the output was out of phase with the given sinusoidal time-varying input signal and there existed tracking error. This control synthesis provided robust trajectory tracking control of LLREs and addressed the challenges of tracking error faced by the previous model-based control approaches.

The model-free control was implemented as an overall system approximation controller. An adaptive PD RBFNN controller was designed. The comparison between the performance parameters of the designed model-based and model-free control strategies is presented.

The tracking performances for the lead compensated H_∞ controller and the adaptive PD RBFNN controller are both effective; however, the response of the model-free controller is faster than that of the model-based controller. Future work will include improvements to the MB and MF control approaches for further optimization of the responses.

Author Contributions: Conceptualization, M.T.S. and S.Q.; methodology, M.T.S. and Z.K.; software, M.T.S.; validation, Z.K., A.M.M. and S.Q.; formal analysis, A.M.M.; investigation, M.T.S.; resources, J.Z.G. and Z.M.U.D.; data curation, A.M.M.; writing—original draft preparation, M.T.S.; writing—review and editing, Z.K.; visualization, A.M.M.; supervision, S.Q.; project administration, M.T.S., J.Z.G. and Z.M.U.D.; funding acquisition, J.Z.G. and Z.M.U.D. All authors have read and agreed to the published version of the manuscript.

Institutional Review Board Statement: Not applicable.

Informed Consent Statement: Not applicable.

Data Availability Statement: Not applicable.

Conflicts of Interest: The authors declare no conflict of interest.

References

1. Chen, B.; Ma, H.; Qin, L.Y.; Gao, F.; Chan, K.M.; Law, S.W.; Qin, L.; Liao, W.H. Recent Developments and Challenges of Lower Extremity Exoskeletons. *J. Orthop. Transl.* **2016**, *5*, 26–37. [CrossRef] [PubMed]
2. Chen, G.; Chan, C.K.; Guo, Z.; Yu, H. A Review on Lower Extremity Assistive Robotic Exoskeleton in Rehabilitation Therapy. *Crit. Rev. Biomed. Eng.* **2013**, *41*, 343–363. [CrossRef] [PubMed]
3. Díaz, I.; Gil, J.J.; Sánchez, E. Lower-Limb Robotic Rehabilitation: Literature Review and Challenges. *J. Robot.* **2011**, *2011*, 759764. [CrossRef]
4. Rupal, B.S.; Rafique, S.; Singla, A.; Singla, E.; Isaksson, M.; Virk, G.S. Lower-limb Exoskeletons: Research Trends and Regulatory Guidelines in Medical and Non-medical Applications. *Int. J. Adv. Robot. Syst.* **2017**, *14*, 1–27. [CrossRef]
5. Pamungkas, D.S.; Caesarendra, W.; Soebakti, H.; Analia, R.; Susanto, S. Overview: Types of Lower Limb Exoskeletons. *Electronics* **2019**, *8*, 1283. [CrossRef]
6. Zhang, F.; Li, P.; Hou, Z.; Xie, X.; Chen, Y.; Li, Q.; Tan, M. An Adaptive RBF Neural Network Control Strategy for Lower Limb Rehabilitation Robot. In Proceedings of the International Conference on Intelligent Robotics and Applications (ICIRA), Shanghai, China, 10–12 November 2010; pp. 417–427.
7. Ma, Y.; He, W.; Ge, S.S. Modeling and Control of a Lower-Limb Rehabilitation Robot. In Proceedings of the 4th International Conference on Social Robotics (ICSR), Chengdu, China, 29–31 October 2012; pp. 581–590.
8. Lu, R.; Li, Z.; Su, C.Y.; Xue, A. Development and Learning Control of a Human Limb with a Rehabilitation Exoskeleton. *IEEE Tranl. Ind. Electron.* **2014**, *61*, 3776–3785. [CrossRef]
9. Zhang, X.; Wang, H.; Tian, Y.; Wang, Z.; Laurent, P. Modeling, Simulation and Control of Human Lower Extremity Exoskeleton. In Proceedings of the 34th Chinese Control Conference, Hangzhou, China, 28–30 July 2015; pp. 6066–6071.
10. Cao, F.; Li, C.; Li, Y. Robust Sliding Mode Adaptive Control for Lower Extremity Exoskeleton. In Proceedings of the Chinese Automation Congress, Wuhan, China, 27–29 November 2015; pp. 400–405.
11. Huang, T.H.; Cheng, C.A.; Huang, H.P. Self-learning Assistive Exoskeleton with Sliding Mode Admittance Control. In Proceedings of the IEEE/RSJ International Conference on Intelligent Robots Systems, Tokyo, Japan, 3–7 November 2013; pp. 698–703.
12. Lv, X.; Yang, C.; Li, X.; Han, J. Passive Training Control for the Lower Limb Rehabilitation Robot. In Proceedings of the IEEE International Conference on Mechatronics and Automation (ICMA), Takamatsu, Japan, 6–9 August 2017; pp. 904–909.
13. Saeed, M.T.; Qin, S. Comprehensive Modeling and Simulation of an Anthropomorphic Robotic Exoskeleton for Rehabilitation. In Proceedings of the 16th International Bhurban Conference on Applied Sciences and Technology, Islamabad, Pakistan, 8–12 January 2019; pp. 347–352.
14. Barjuei, E.S.; Toxiri, S.; Medrano-Cerda, G.A.; Caldwell, D.G.; Ortiz, J. Bond Graph Modeling of an Exoskeleton Actuator. In Proceedings of the 10th Computer Science and Electronic Engineering Conference, Colchester, UK, 19–21 September 2018; pp. 101–106.
15. Radu, I.; Cătălin, U. Lagrange's Equations versus Bond Graph Modeling Methodology by an Example of a Mechanical System. *Appl. Mech. Mater.* **2015**, *809–810*, 914–919.
16. Nguyen, L.; Ramakrishnan, J.; Granda, J. International Space Station Centrifuge Rotor Models. A Comparison of the Euler-Lagrange and the Bond Graph Modeling Approach. In Proceedings of the International Conference on Bond Graph, San Diego, CA, USA, 15–17 January 2007; pp. 1–8.

17. Shojaei Barjuei, E.; Caldwell, D.G.; Ortiz, J. Bond Graph Modeling and Kalman Filter Observer Design for an Industrial Back-Support Exoskeleton. *Designs* **2020**, *4*, 53. [CrossRef]
18. Jain, P.; Bera, T.K.; Rafique, S.; Singla, A.; Isaksson, M. Comparative study of knee joint torque estimations for linear and rotary actuators using bond graph approach for stand–sit–stand motions. *Int. J. Adv. Robot. Syst.* **2020**, *17*, 1–13. [CrossRef]
19. Oh, S.; Baek, E.; Song, S.K.; Mohammad, S.; Jeon, D.; Kong, K. A Generalized Control Framework of Assistive Controllers and its Application to Lower Limb Exoskeletons. *Robot. Auton. Syst.* **2015**, *73*, 68–77. [CrossRef]
20. Shi, L.; Fu, L.; Liu, Z. Model-Based Active Impedance Controller Development of the Exoskeleton Rehabilitation Robot (ERRobot) For Lower-Extremity. In Proceedings of the IEEE Smart World, Ubiquitous Intelligence & Computing, Advanced & Trusted Computing, Scalable Computing & Communications, Cloud & Big Data Computing, Internet of People and Smart City Innovation (SmartWorld/SCALCOM/UIC/ATC/CBDCom/IOP/SCI), Guangzhou, China, 8–12 October 2018; pp. 150–155.
21. Do, T.; Vu, D.T. A Simple Control Method for Exoskeleton for Rehabilitation. *Int. J. Elect. Electr. Eng.* **2017**, *4*, 7–12. [CrossRef]
22. Yang, Z.; Zhu, Y.; Yang, X.; Zhang, Y. Impedance Control of Exoskeleton Suit Based on RBF Adaptive Network. In Proceedings of the IEEE International Conference on Intelligent Human-Machine Systems and Cybernetics (IHMSC), Hangzhou, China, 26–27 August 2009; pp. 182–187.
23. Ashrafiuon, H.; Grosh, K.; Burke, K.J.; Bommer, K. An Intelligent Exoskeleton for Lower Limb Rehabilitation. In Proceedings of the ASME International Design Engineering Technical Conference & Computers and Information in Engineering Conference, Montreal, QC, Canada, 15–18 August 2010; pp. 3–9.
24. Cao, F.; Li, Y.; Shi, J. Adaptive Sliding Mode Impedance Control in Lower Limbs Rehabilitation Robotic. In Proceedings of the Chinese Automation Congress, Changsha, China, 7–8 November 2013; pp. 310–315.
25. Majeed, A.P.P.A.; Taha, Z.; Abidin, A.F.Z.; Zakaria, M.A.; Khairuddina, I.M.; Razman, M.A.M.; Mohamed, Z. The Control of a Lower Limb Exoskeleton for Gait Rehabilitation: A Hybrid Active Force Control Approach. *Procedia Comp. Sci.* **2016**, *105*, 183–190. [CrossRef]
26. Shahi, H.; Yousefi-Koma, A.; Moghaddam, M.M. Robust Adaptive Admittance Control of an Exoskeleton in the presence of Structured and Unstructured Uncertainties. *Adv. Robot.* **2018**, *32*, 242–265. [CrossRef]
27. Beyl, P.; Van Damme, M.; Van Ham, R.; Vanderborght, B.; Lefeber, D. Design and Control of a Lower Limb Exoskeleton for Robot-assisted Gait Training. *Appl. Bionics Biomech.* **2009**, *26*, 229–243. [CrossRef]
28. Kikuuwe, R.; Fujimoto, H. Proxy-Based Sliding Mode Control for Accurate and Safe Position Control. In Proceedings of the IEEE International Conference on Robotics and Automation, Orlando, FL, USA, 15–19 May 2006; pp. 25–30.
29. Jezernik, S.; Colombo, G.; Morari, M. Joint-Angle Trajectory Adaptation for the Robotic Orthosis Lokomat. In Proceedings of the Workshop on European Scientific and Industrial Collaboration, Enschede, The Netherlands, 27–29 June 2001; pp. 451–456.
30. Jezernik, S.; Pfister, A.; Frueh, H.; Colombo, G.; Morari, M. Robotic Orthosis Lokomat: Its use in the Rehabilitation of Locomotion and in the Development of the Biology-based Neural Controller. *Neuromodulation* **2003**, *6*, 108–115. [CrossRef]
31. Wu, J.; Gao, J.; Song, R.; Li, R.; Li, Y.; Jiang, L. The design and control of a 3DOF lower limb rehabilitation robot. *Mechatronics* **2016**, *33*, 13–22. [CrossRef]
32. Pan, D.; Gao, F.; Miao, Y.; Cao, R. Co-simulation Research of a Novel Exoskeleton-human Robot System on Humanoid Gaits with Fuzzy-PID/PID Algorithms. *Adv. Eng. Softw.* **2015**, *79*, 36–46. [CrossRef]
33. Koceska, N.; Koceski, S.; Durante, F.; Zobel, P.B.; Raparelli, T. Control Architecture of a 10 DOF Lower Limbs Exoskeleton for Gait Rehabilitation. *Int. J. Adv. Robot. Syst.* **2013**, *10*, 68. [CrossRef]
34. Zhang, X.; Wang, H.; Tian, Y.; Peyrodie, L.; Wang, X. Model-free based Neural Network Control with Time-delay Estimation for Lower Extremity Exoskeleton. *Neurocomputing* **2018**, *272*, 178–188. [CrossRef]
35. Liu, D.; Tang, Z.; Pei, Z. The Motion Control of Lower Extremity Exoskeleton Based on RBF Neural Network Identification. In Proceedings of the IEEE International Conference on Information and Automation, Lijiang, China, 8–10 August 2015; pp. 1838–1842.
36. Ferris, D.P.; Lewis, C.L. Robotic Lower Limb Exoskeletons Using Proportional Myoelectric Control. In Proceedings of the Annual International Conference of the IEEE Engineering in Medicine and Biology Society, Minneapolis, MN, USA, 23–27 July 2009; pp. 2119–2124.
37. McDaid, A.J.; Xing, S.; Xie, S.Q. Brain Controlled Robotic Exoskeleton for Neurorehabilitation. In Proceedings of the IEEE/ASME International Conference on Advanced Intelligent Mechatronics, Wollongong, NSW, Australia, 9–12 July 2013; pp. 1039–1044.
38. Yin, Y.H.; Fan, Y.J.; Xu, L.D. EMG and EPP-Integrated Human–Machine Interface between the Paralyzed and Rehabilitation Exoskeleton. *IEEE Trans. Inform. Technol. Biomed.* **2012**, *16*, 542–549. [CrossRef]
39. Ghezal, M.; Guiatni, M.; Boussioud, I.; Renane, C.S. Design and Robust Control of a 2 DOFs Lower Limb Exoskeleton. In Proceedings of the International Conference on Communications and Electrical Engineering, El Oued, Algeria, 17–18 December 2018; pp. 1–6.
40. Yin, G.; Zhang, X.; Chen, J.; Shi, Q. RBF Neural Network Compensation based Trajectory Tracking Control for Rehabilitation Training Robot. In Proceedings of the IEEE International Conference on Cyber Technology in Automation, Control and Intelligent Systems, Shenyang, China, 8–12 June 2015; pp. 359–364.
41. Cui, C.; Bian, G.B.; Hou, Z.G.; Tan, M.; Zhang, D.; Xie, X.L.; Wang, W. An RBF-Based Neuro-Adaptive Control Scheme to Drive a Lower Limb Rehabilitation Robot. In Proceedings of the IEEE International Conference on Robotics and Biomimetics, Zhuhai, China, 6–9 December 2015; pp. 397–402.

42. Yu, L.; Fei, S.; Huang, J.; Gao, Y. Trajectory Switching Control of Robotic Manipulators Based on RBF Neural Networks. *Circuits Syst. Signal Process.* **2014**, *33*, 1119–1133. [CrossRef]

43. Daachi, M.E.; Madani, T.; Daachi, B.; Djouani, K. A Radial Basis Function Neural Network Adaptive Controller to drive a Powered Lower Limb Knee Joint Orthosis. *Appl. Soft Comput.* **2015**, *34*, 324–336. [CrossRef]

44. Yang, Y.; Huang, D.; Dong, X. Enhanced Neural Network Control of Lower Limb Rehabilitation Exoskeleton by Add-on Repetitive Learning. *Neurocomputing* **2019**, *323*, 256–264. [CrossRef]

45. Chen, Z.; Guo, Q.; Yan, Y.; Jiang, D. Robust Sliding Mode Control for a 2-DOF Lower Limb Exoskeleton Base on Linear Extended State Observer. *J. Mech. Eng. Sci.* **2020**, *2*, 1–6. [CrossRef]

46. Saeed, M.T.; Qin, S. Robust Control of a Mechatronic Exoskeleton for Motion Rehabilitation. In Proceedings of the IEEE International Conference on Mechatronics and Automation, Tianjin, China, 4–7 August 2019; pp. 998–1003.

47. Zhou, K.; Doyle, J.C. H_∞ Control. In *Essentials of Robust Control*, 1st ed.; Prentice Hall: Upper Saddle River, NJ, USA, 1997; pp. 269–291.

48. Burl, J.B. Robustness and Full Information Control and Estimation. In *Linear Optimal Control H_2 and H_∞ Methods*; Addison-Wiesley: Boston, MA, USA, 1999; pp. 330–348.

49. Zhang, M.G.; Li, W.H.; Liu, M.Q. Adaptive PID Control Strategy Based on RBF Neural Network Identification. In Proceedings of the International Conference on Neural Networks and Brain, Beijing, China, 13–15 October 2005; pp. 1854–1857.

50. Song, S.; Zhang, X.; Tan, Z. RBF Neural Network Based Sliding Mode Control of a Lower Limb Exoskeleton Suit. *J. Mech. Eng.* **2014**, *60*, 437–446. [CrossRef]

51. Jinkun, L. *Radial Basis Function (RBF) Neural Network Control for Mechanical Systems Design, Analysis and MATLAB Simulation*; Tsinghua University Press: Beijing, China; Springer: Berlin/Heidelberg, Germany, 2013; pp. 79–83.

52. Wang, L.-X. *A Course in Fuzzy Systems and Control*; Prentice Hall International Inc.: Hoboken, NJ, USA, 1996; pp. 305–306.